Supporting Information

Environmentally friendly luminescent solar concentrators based on optically efficient and stable green fluorescent protein

Carlota P. A. Carlos,[1,2] Sandra F. H. Correia,[1] Margarida Martins,[3] Oleksandr A. Savchuk,[2] João A. P. Coutinho,[3] Paulo S. André,[4] Jana B. Nieder,[2] Sónia P. M. Ventura,[3] Rute A. S. Ferreira[1]*

[1]Phantom-G, Department of Physics and CICECO – Aveiro Institute of Materials, University of Aveiro, 3810-193 Aveiro, Portugal,
[2]Department of Nanophotonics, Ultrafast Bio- and Nanophotonics group, INL - International Iberian Nanotechnology Laboratory, Av. Mestre José Veiga s/n, 4715-330, Braga, Portugal
[3]Department of Chemistry and CICECO – Aveiro Institute of Materials, University of Aveiro, 3810-193 Aveiro, Portugal
[4]Department of Electrical and Computer Engineering and Instituto de Telecomunicações, Instituto Superior Técnico, Universidade de Lisboa, 1049-001 Lisbon, Portugal
Corresponding E-mail: rferreira@ua.pt

Contents:

Table S1. Emission quantum yield (*q*) values of the d-U(600) doped with eGFP according to the excitation wavelength (λ_{exc}). The associated error is 10%.

λ_{exc} [nm]	360	370	380	390	400	410	420	430	440	450	460	470	480	490	500
q	0.06	0.06	0.06	0.06	0.08	0.08	0.09	0.11	0.14	0.18	0.22	0.31	0.31	0.33	0.31

Table S2. Molar extinction coefficient (*ε)*, absolute emission quantum yield (*q*) and brightness (*B*) of distinct reported materials.

Material	**ε (×10⁴) [M⁻¹ cm⁻¹]**	***q***	***B* (×10⁴) [M⁻¹ cm⁻¹]**	**Reference**
R-phycoerythrin aqueous solution	140	0.30	40	1
Wild-type GFP	2.1	0.77	1.6	2
SiR	9.3	0.41	3.8	3
Rh_QCO_2H	7.0	0.79	5.5	3
530RH	5.6	0.89	5.0	3
560CP	6.1	0.76	4.6	3
6-ROX	8.2	0.76	6.2	3
575RH	5.5	0.74	4.1	3
GeR	9.7	0.43	4.2	3
630GeRH	6.1	0.60	3.7	3
640SiRH	5.1	0.42	5.5	3
Eu^{3+}-functionalized ionosilicas/PMMA	0.20	0.52	0.1	4
	11	0.301	3.8	5
Tb^{3+}-functionalized ionosilicas/PMMA	22	0.02	0.35	5

PMMA= poly(methyl methacrylate)

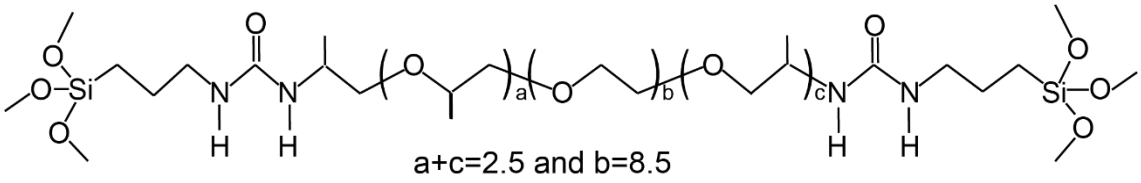

Figure S1. Molecular structure of the di-ureasil organic-inorganic hybrid, d-U(600).

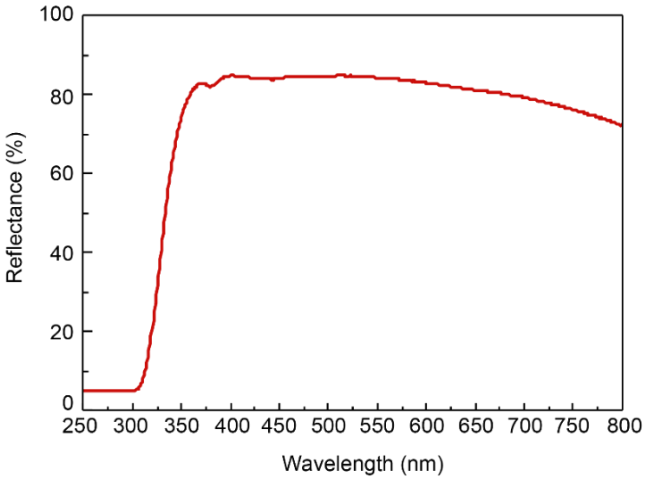

Figure S2. Reflectance curve of the reflective tape used on the LSCs.

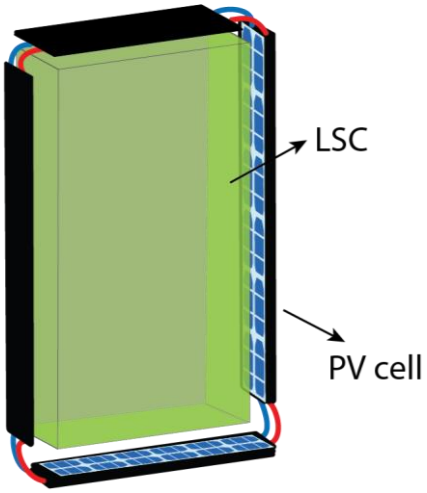

Figure S3. Schematic representation of the p-LSCs based on a glass container filled with eGFP with concentration of 5.5×10^{-5} M, with PV cells located at all the edges.

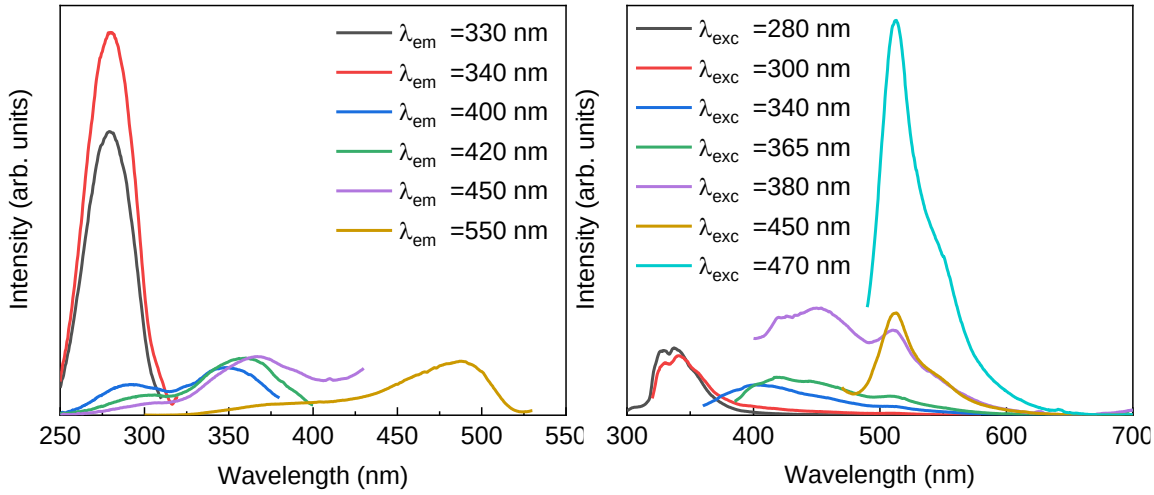

Figure S4. Room temperature excitation (left) and emission (right) of the eGFP-doped d-U(600) organic-inorganic hybrid monitored (λ_{em}) and excited (λ_{exc}) at distinct wavelengths, respectively.

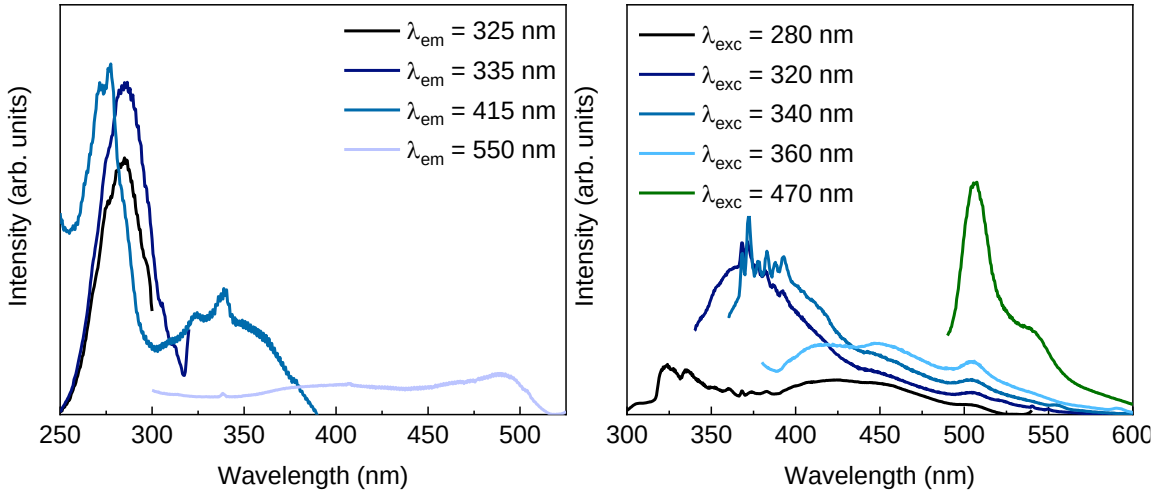

Figure S5. Low temperature excitation (left) and emission (right) of the eGFP-doped d-U(600) organic-inorganic hybrid monitored (λ_{em}) and excited (λ_{exc}) at distinct wavelengths, respectively, measured at 13 K.

The spectra measured at 13 K (Fig. S3) show an increase in the relative intensity of the hybrid emission when compared to the spectra at room temperature. The characteristic emission peak of eGFP is detected for all the selected excitation wavelengths and is blue shifted in comparison to that of the hybrid at room temperature, peaking at 505 nm with a shoulder at 538 nm. A temperature-dependent spectral broadening is verified: at room temperature this peak is broader (FWHM~40 nm) than the one at 13 K (FWHM~26 nm). This is in agreement to the literature, where the eGFP emission is reported to blue shift and become narrower at lower temperatures due to the temperature dependence of the I excited state.[6, 7] The excitation peak around 488 nm is also narrower at 13 K than at room temperature, supporting the hypothesis that the shift and narrowing of eGFP emission is due to the depopulation of the I excited state.

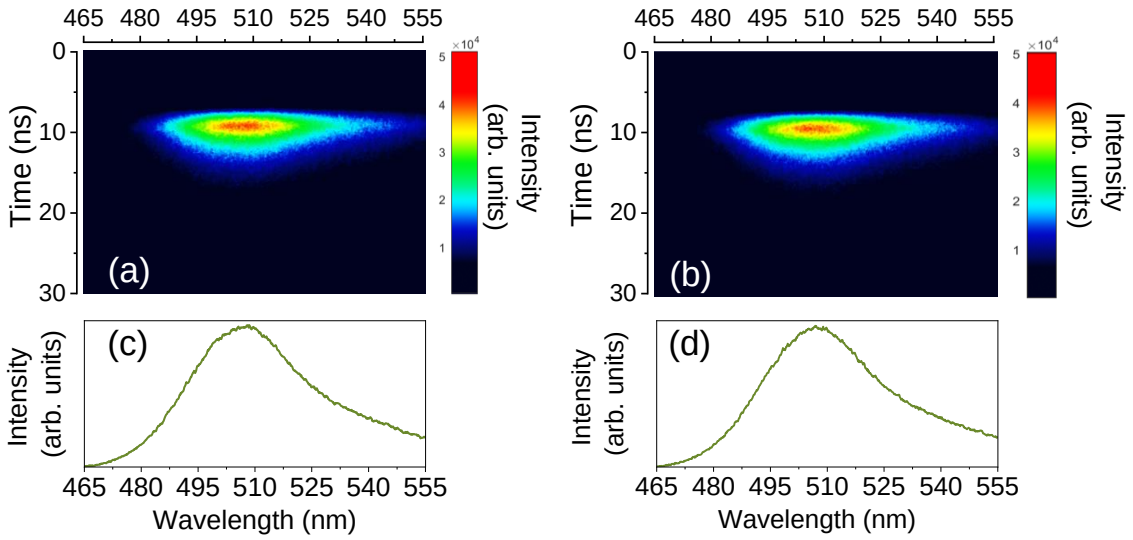

Figure S6. Streak images recorded for (a) 1.3×10^{-5} M and (b) 3.5×10^{-5} M the eGFP aqueous solutions. Next to each figure is placed the respective intensity colourbar. The respective integrated fluorescence emission spectra, (c) and (d), are shown on the bottom.

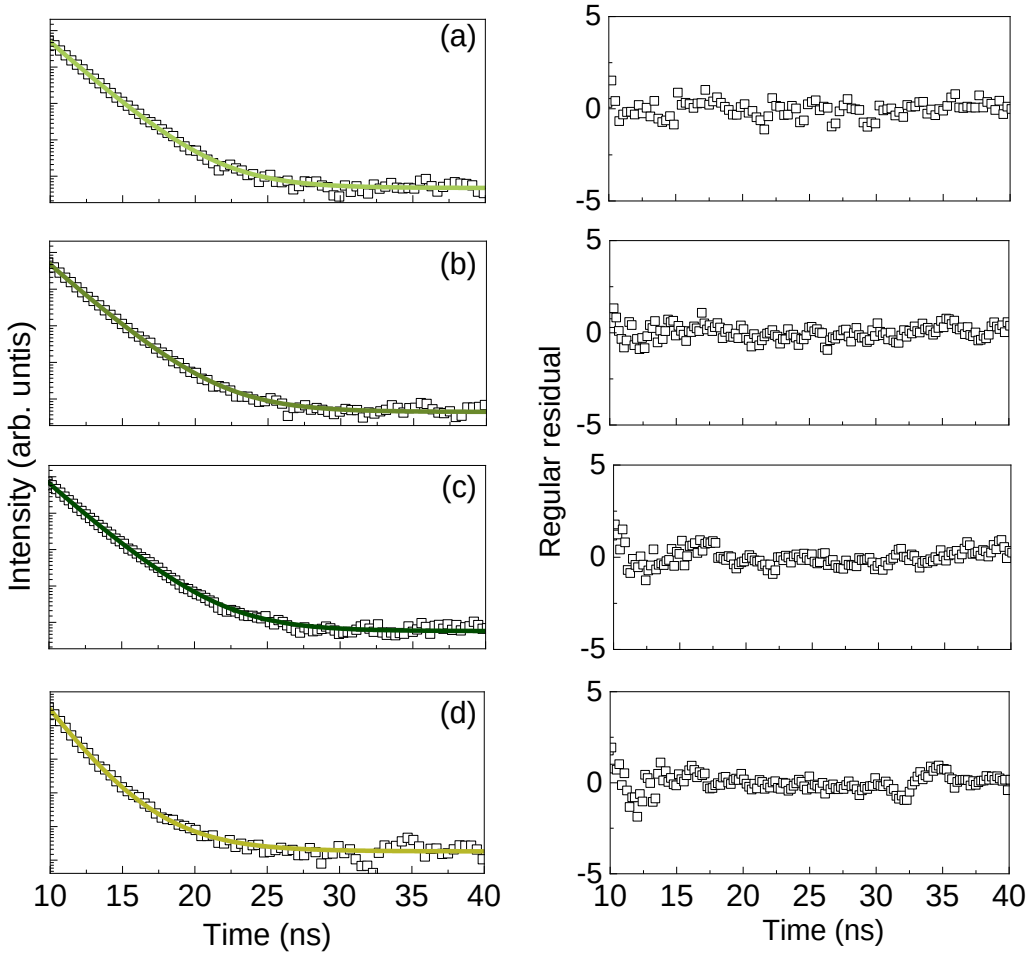

Figure S7. Streak-based fluorescent decay curves measured for the three eGFP solutions, (a) 1.4×10^{-5} M, (b) 3.5×10^{-5} M and (c) 5.5×10^{-5} M solutions, and for the (d) eGFP-doped d-U(600) hybrid sample, plotted with a logarithmic y-axis. The correspondent regular residual of the single exponential function fitted to the data ($R^2 > 0.99$) are aside each plot.

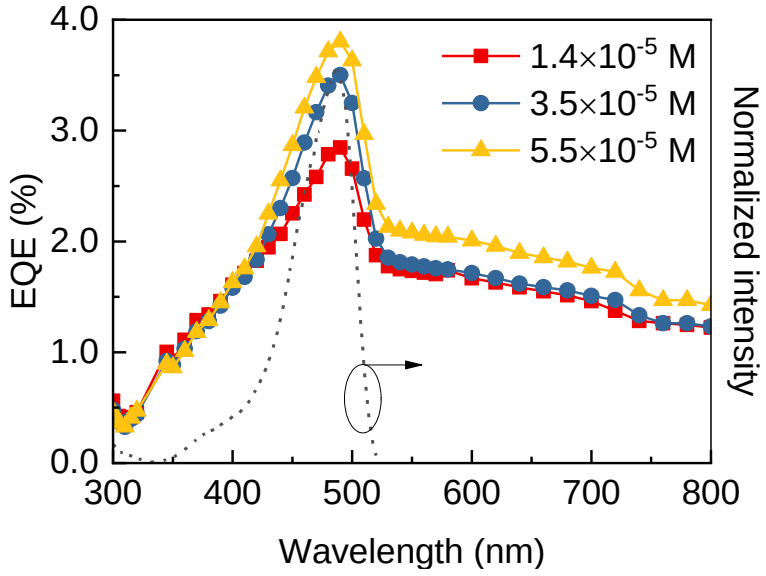

Figure S8. EQE values calculated for the p-LSCs based on eGFP aqueous solutions. The dashed line represents the excitation spectra of the solutions (right *y* axis).

eGFP-doped d-U(600) LSC

The LSC based on eGFP-doped d-U(600) organic-inorganic hybrid (Figure S1) was characterized similarly to the LSCs based on the aqueous solutions. The maximum η_{opt} value of 3.7±0.1% is like the one found for the p-LSCs based on the eGFP aqueous solutions. Also, in this case, the EQE values were calculated between 300–800 nm (Figure S7), yielding a maximum value of ~0.32%. The shoulder between 450 and 520 nm ascribed to eGFP absorption is not evident for the bulk prototype, when compared to the pronounced shoulder recorded for the liquid p-LSCs. However, the emission spectrum at the edge of the monolith where the PV cell is placed (Figure S8) showed the emission peak at 515 nm attributed to eGFP emission, confirming that the incident solar radiation is being absorbed by the eGFP molecules incorporated in the organic-inorganic hybrid and then re-emitted and collected at the edges of the p-LSC.

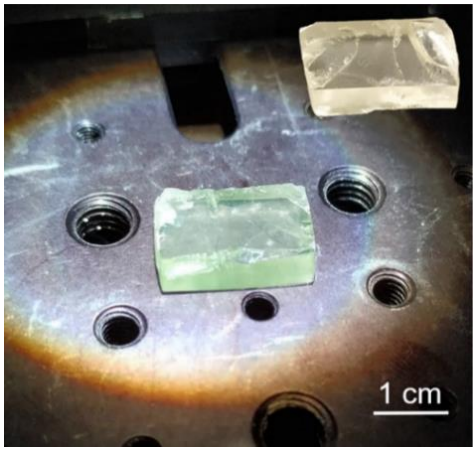

Figure S9. Photograph of the p-LSC based on the d-U(600) hybrid doped with eGFP under AM1.5G illumination. The inset shows the same LSC under daylight illumination.

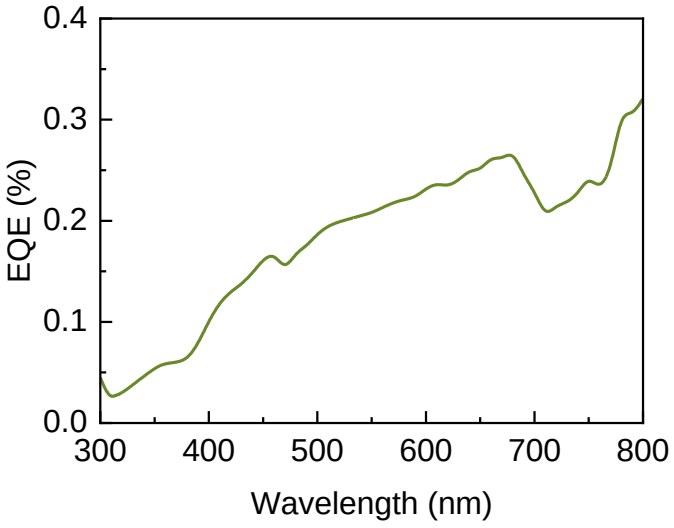

Figure S10. EQE values calculated for the p-LSC based on the d-U(600) organic-inorganic hybrid doped with eGFP.

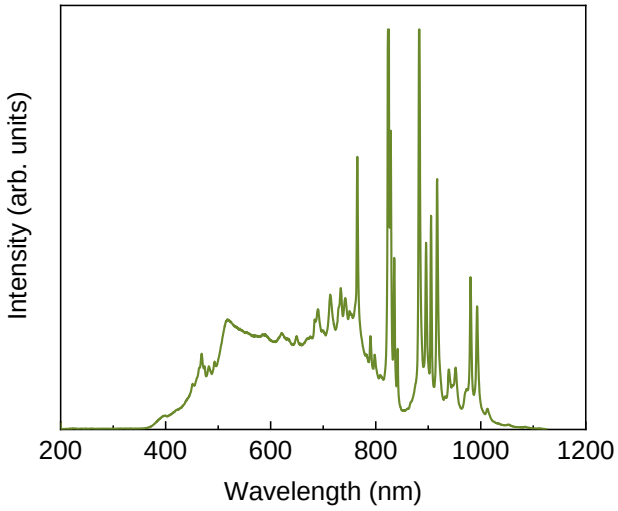

Figure S11. Emission spectra recorded at the edge of the p-LSC based on the d-U(600) organic-inorganic hybrid doped with eGFP.

1. A. R. Frias, S. F. H. Correia, M. Martins, S. P. M. Ventura, E. Pecoraro, S. L. Ribeiro, P. S. Andre, R. A. S. Ferreira, J. A. P. Coutinho and L. D. Carlos, *Adv. Sustain. Syst.*, 2019, **3**, 1800134.
2. R. Heim and R. Y. Tsien, *Curr. Biol.*, 1996, **6**, 178-182.
3. A. N. Butkevich, V. N. Belov, K. Kolmakov, V. V. Sokolov, H. Shojaei, S. C. Sidenstein, D. Kamin, J. Matthias, R. Vlijm, J. Engelhardt and S. W. Hell, *Chem.-Eur. J.*, 2017, **23**, 12114-12119.
4. M. A. Cardoso, S. F. H. Correia, A. R. Frias, H. Gonçalves, R. F. P. Pereira, S. C. Nunes, M. Armand, P. S. André, V. de Zea Bermudez and R. A. S. Ferreira, *J. Rare Earth*, 2020, **38**, 531-538.
5. A. R. Frias, M. A. Cardoso, A. R. N. Bastos, S. F. H. Correia, P. S. Andre, L. D. Carlos, V. D. Bermudez and R. A. S. Ferreira, *Energies*, 2019, **12**, 451.
6. T. M. H. Creemers, A. J. Lock, V. Subramaniam, T. M. Jovin and S. Volker, *Nat. Struct. Biol.*, 1999, **6**, 557-560.
7. P. Leiderman, D. Huppert and N. Agmon, *Biophys. J.*, 2006, **90**, 1009-1018.